Modulation of H-NS transcriptional silencing by magnesium

W. Ryan Will[1], Patrick J. Whitham[2], Philip J. Reid[2] and Ferric C. Fang[1,3,*]

[1]Department of Laboratory Medicine, University of Washington School of Medicine, Seattle, WA 98195, USA,
[2]Department of Chemistry, University of Washington, Seattle, WA 98195, USA and [3]Department of Microbiology,
University of Washington School of Medicine, Seattle, WA 98195, USA

ABSTRACT

The bacterial histone-like protein H-NS silences AT-rich DNA, binding DNA as 'stiffened' filaments or 'bridged' intrastrand loops. The switch between these modes has been suggested to depend on the concentration of divalent cations, in particular Mg^{2+}, with elevated Mg^{2+} concentrations associated with a transition to bridging. Here we demonstrate that the observed binding mode is a function of the local concentration of H-NS and its cognate binding sites, as well as the affinity of the interactions between them. Mg^{2+} does not control a binary switch between these two modes but rather modulates the affinity of this interaction, inhibiting the DNA-binding and silencing activity of H-NS in a continuous linear fashion. The direct relationship between conditions that favor stiffening and transcriptional silencing activity suggests that although both modes can occur in the cell, stiffening is the predominant mode of binding at silenced genes.

INTRODUCTION

The histone-like nucleoid structuring protein H-NS plays a pivotal role in gene regulation and in the evolution of α-, β- and γ-proteobacteria such as *Salmonella enterica* by serving as a xenogeneic silencer that can bind and repress AT-rich DNA sequences (1,2). Xenogeneic silencing allows the recipients of newly-acquired genes to avoid adventitious effects of unregulated gene expression and to integrate horizontally-acquired genes into existing regulatory networks (3). H-NS exhibits two critical features required for its role as a xenogeneic silencer. The first is an ability to recognize DNA with relatively increased AT-content via a Q/RGR or AT-hook motif (4), which recognizes the unique minor groove conformation of AT-rich DNA, in particular 'TpA steps' that create a kink in the DNA backbone.

The second feature is the presence of an amino-terminal oligomerization domain, which allows H-NS to oligomerize in both head-to-head and tail-to-tail orientations, forming chains when bound to DNA (5–11). H-NS nucleation at high-affinity TpA sites can be followed by lateral oligomerization across long stretches of DNA to silence gene expression. H-NS–DNA oligomeric silencing complexes provide large regulatory targets that can be relieved by competing counter-silencing mechanisms to control gene expression. The architectural flexibility of counter-silencing appears to be evolutionarily favored over the precise structural constraints required by RNA polymerase for canonical activation (3,12).

Although recent studies have provided significant insights into H-NS–DNA interactions, details of the higher-order structure of silencing complexes remain unclear due to conflicting lines of evidence regarding the mode of DNA binding by H-NS. Initial atomic force microscopy studies suggested that H-NS forms loops between relatively distant DNA regions as a result of its multiple dimerization domains (13,14), termed the 'bridging' mode of binding. However, biophysical studies have shown that an H-NS–DNA complex forms stiffened filaments (15), termed the 'stiffening' mode of binding. Liu *et al.* (16) subsequently demonstrated that both binding modes could be observed *in vitro*, and suggested that the switch between the two distinctive binding modes is controlled by divalent cation concentrations. Under low (<2 mM) Mg^{2+} concentrations, stiffening appears to be the predominant binding mode, whereas higher (≥5 mM) Mg^{2+} concentrations are thought to promote bridging. Although the intracellular Mg^{2+} concentration is estimated to be 100 mM (17), most of this Mg^{2+} is sequestered by cellular components such as ribosomes. As a result, the concentration of free intracellular Mg^{2+} is thought to be approximately 1–2 mM (18,19). It is therefore conceivable that either stiffening or bridging modes of H-NS binding might be physiologically relevant, and previous studies have argued for regulatory roles of both binding modes. Lim *et al.* (20) demonstrated that mutant H-NS

*To whom correspondence should be addressed. Tel: +1 206 221 6770; Fax: +1 206 616 1575; Email: fcfang@u.washington.edu
Present address: Patrick J. Whitham, Applied Physics Laboratory, University of Washington, Seattle, WA 98195, USA.

proteins that are unable to form filaments *in vitro* are also unable to function as silencers *in vivo*, suggesting that the stiffening mode is required for silencing. However, bridging has been shown to promote RNA polymerase (RNAP) pausing *in vitro* (21), suggesting a regulatory role for this binding mode as well.

The goal of the present study was to establish the H-NS binding mode relevant to transcriptional silencing and to clarify the role of divalent cation concentrations on H-NS actions. A model H-NS-silenced regulatory circuit based on the horizontally-acquired *Salmonella enterica pagC* promoter (12,22) was reconstituted using Mg^{2+} concentrations associated with promoting either stiffening (1 mM) or bridging (10 mM) modes of binding. Biochemical and biophysical assays were performed to assess the structure and activity of the H-NS–DNA complex under these conditions.

MATERIALS AND METHODS

DNA and protein purification

All experiments were performed using pRW6 (12), consisting of a 2.7 kb fragment of the *S.* Typhimurium 14028s chromosome containing the complete *pagC* promoter and coding sequence, as well as the coding sequences of upstream and downstream genes (Supplementary Figure S1), inserted into the low copy vector, pWKS30 (23), which was purified with a Qiagen Midi (Qiagen, Valencia, CA, USA), using the manufacturer's protocol for very low copy plasmids. DNA was then extracted twice with phenol:$CHCl_3$:IAA (25:24:1), ethanol precipitated, and dissolved in 10 mM Tris–HCl (pH 8.0). H-NS was purified as an N-terminal 6xHis-tagged protein as previously described (12).

In vitro transcription

Reactions were performed as previously described (12), with the following changes: Reactions were assembled in IVT buffer containing 40 mM HEPES, pH 7.3, 60 mM potassium glutamate, 0.5 mM $CaCl_2$, 1 mM DTT, 0.05% NP-40, 0.1 mg ml^{-1} BSA and 10% glycerol to a final volume of 20 µl. $MgCl_2$ was added to the indicated concentration, followed by addition of pRW6 to a final concentration of 1 nM and 20 U of RNasin (Promega, Madison, WI, USA). Reactions were allowed to equilibrate for 10 min at 37°C before the addition of H-NS to the indicated concentration. Reactions were incubated for an additional 10 min at 37°C before adding RNAP (Epicentre, Madison, WI, USA) to a final concentration of 10 nM. Reactions were incubated at 37°C for 10 min before adding rNTPs to a final concentration of 2 mM. Reactions were then completed by incubating for 10 min at 37°C, allowing transcription to initiate continuously and terminate at intrinsic rho-independent terminators. Reactions were stopped by adding 20 µl of DNase I buffer and incubating at 37°C for 30 min, followed by 5 min of incubation at 65°C. Reactions were diluted 1:100 and reverse transcribed using the Qiagen QuantiTect Reverse Transcription Kit (Qiagen, Valencia, CA, USA) with the sequence and strand-specific probe pagC-3′-P (5′-TGTAGAGGAGATGTTGCTTCC-3′) in 10 µl reactions following the manufacturer's instructions. The resulting cDNA was quantified by qPCR in 20 µl SYBR Green master mix (24) on a BioRad CFX 96 (BioRad, Hercules, CA) using the primers pagC-3′-F (5′-AGAACATTCCACT CAGGATGGCGA-3′) and pagC-3′-R (5′- GACGACGA TATTCTCCAGCGGATT-3′), generating a 112 bp amplicon. The specificity of each reaction was confirmed via melt curve analysis.

DNase I and UV laser footprinting

DNase I footprinting reactions were assembled in IVT buffer to a final volume of 20 µl with 1 nM pRW6 and $MgCl_2$ was added to the indicated concentration. Reactions were equilibrated at 37°C for 10 min, H-NS was added to the indicated concentration, and reactions were incubated at 37°C for an additional 10 min. After the addition of 0.002 U of DNase I, digestion was allowed to proceed for 2 min at 37°C before stopping the reaction with 180 µl cold stop buffer containing 330 mM sodium acetate (pH 7.0), 20 mM EDTA and 0.5% sarkosyl. Reactions were then purified, quantified with the 6FAM-pagC probe (5′-6FAM-A CTTGTGAGTTCATCTCCTGAATTATGG-3′) and analyzed via DDFA as previously described (12).

UV laser footprinting reactions were assembled as described above, but the reactions were performed at room temperature. H-NS–DNA complexes were then exposed to an average of one 10 ns pulse of 266 nm UV radiation with an output pulse energy of ∼10 mJ and purified, quantified with the 6FAM-pagC probe, and analyzed as previously described (12).

Atomic force microscopy

Atomic force microscopy (AFM) was performed on a Bruker Dimension Icon (Bruker, Billerica, MA, USA) at the Molecular Analysis Facility at the University of Washington. The 2.7 kb *pagC* target fragment was generated by PCR using the primers pagC2.7F (5′-AGGCGCACT ATACACGTCAGGAAA-3′) and pagC2.7R (5′-GATTT CGTTTATGGCCTGGGGATTT-3′), agarose gel purified and ethanol precipitated to remove excess salt. Mica was functionalized with APTES using the evaporation method (25) and then cured for 2 days under argon. The resulting AP-mica was then modified with 0.5% glutaraldehyde (26), washed with H_2O, and allowed to dry under argon before samples were applied. 200 or 800 nM H-NS was bound to 2 ng/µl *pagC* target at room temperature in AFM binding buffer containing 40 mM HEPES, pH 7.3, 100 mM potassium glutamate and either 1 or 10 mM $MgCl_2$, as indicated. Samples were applied to the glutaraldehyde-modified mica and allowed to bind for 10 min before washing with H_2O and then allowed to dry for at least 2 h under argon. Samples were imaged in air using a ScanAsyst air tip (Bruker).

Light scattering

Light scattering reactions were assembled in AFM binding buffer containing either 1 or 50 mM $MgCl_2$, as indicated, to a final volume of 120 µl. Where indicated, the 2.7 kb *pagC* target fragment used for AFM was added to a concentration of 2 ng/µl. H-NS was added where indicated to a final concentration of 800 nM, and reactions were incubated

at room temperature for 30 min. The absorbance for each sample was measured on a Shimadzu UV-1700 spectrophotometer (Shimadzu, Kyoto, Japan).

Fluorescence anisotropy

Fluorescence anisotropy experiments were performed using a 36 bp DNA molecule formed by annealing two complementary oligonucleotides, 6FAM-HAhnsBS-F (5′-6-FAM-ATGGGTTTTATAGCGAAATAGACTT TTTTATCGCGT-3′) and HAhnsBS-R (5′-ACGCGATA AAAAAGTCTATTTCGCTATAAAACCCAT-3′). The oligonucleotides were combined at a final concentration of 50 μM, incubated at 95°C for 5 min, and then cooled at a rate of 0.1°C/s to allow the formation of a stable duplex. Fluorescence anisotropy experiments were assembled in AFM binding buffer containing 2 nM DNA and either 1 or 10 mM $MgCl_2$, as indicated, to a final volume of 100 μl. H-NS was added at a range of concentrations between 10 and 1000 nM, and the reactions were allowed to equilibrate for 30 min at room temperature. Reactions were analyzed on a Tecan Safire II (Tecan, Männendorf, Switzerland).

RESULTS AND DISCUSSION

H-NS-mediated silencing is dependent on Mg^{2+} concentration

The entire *pagC* coding sequence and flanking genes were included in a 2.7 kb insertion on a low-copy plasmid, which was used for all transcription and footprinting studies (Supplementary Figure S1). The use of a large target region maintains genomic context, and insertion in a low-copy plasmid vector allows the performance of biochemical and functional assays on a supercoiled DNA template. Our experimental design contrasts with previous studies of H-NS binding, both in the effort taken to maintain genomic and structural context, and in the use of a true H-NS-regulated template to allow a direct correlation of binding with transcriptional activity, whereas other studies have typically examined bulk H-NS–DNA interactions with large DNA targets such as the λ bacteriophage (16), pUC19 plasmid (13), calf thymus DNA (27), or artificial constructs fusing noncognate promoters to H-NS-binding sites (21). *In vitro* transcription (IVT) reactions were performed with *pagC* incubated in the presence of increasing concentrations of H-NS and either high (10 mM) or low (1 mM) Mg^{2+} concentrations (Figure 1A). H-NS is a potent transcriptional silencer in 1 mM Mg^{2+}, inhibiting *pagC* transcription 218-fold when present at a concentration of 500 nM, but repression decreased to only 9-fold in 10 mM Mg^{2+}, suggesting that increasing divalent cation concentrations inhibit H-NS-mediated repression. While it is possible that H-NS may inhibit both transcription initiation and elongation, we have previously shown that RNAP is unable to bind the silenced *pagC* promoter (12), indicating that repression of *pagC* likely occurs at the level of transcription initiation. To exclude the effects of Mg^{2+} concentration on RNAP activity, the relative repression at each H-NS concentration was normalized to the baseline transcriptional activity of RNAP. Although RNAP activity appears to decrease modestly (∼4-fold) at low Mg^{2+} concentrations (<5 mM Mg^{2+})
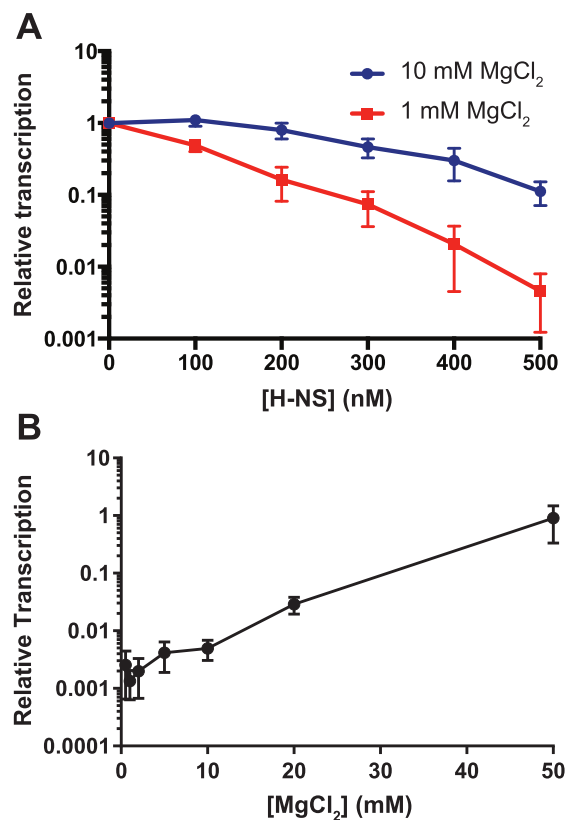
Figure 1. H-NS-mediated silencing is inhibited by increasing Mg^{2+} concentrations. (**A**) IVT was performed on *pagC* template with increasing concentrations of H-NS under either stiffening (1 mM $MgCl_2$; red line) or bridging (10 mM $MgCl_2$; blue line) conditions. Reactions are normalized to the 0 nM reaction. To determine if H-NS exhibits a binary response to Mg^{2+}, IVT was performed on *pagC* template in the presence of 500nM H-NS and increasing concentrations of $MgCl_2$ (**B**). Transcript quantities were normalized to an H-NS-free control reaction for each concentration of $MgCl_2$ (see Supplementary Figure S3 for pre-normalization and control data). Data represent the mean ± SEM; $n = 3$.

(Figure 1B; Supplementary Figure S2), this effect is insufficient to account for the degree of repression exhibited by H-NS. These observations indicate that H-NS is most active under conditions associated with stiffening, i.e. low Mg^{2+} concentrations.

Given these observations, the two-mode binding model (16) suggests that H-NS silencing activity should exhibit a binary response to increasing Mg^{2+} concentrations, transitioning between two relatively stable levels of activity at ∼5 mM Mg^{2+}. To test this hypothesis, we performed IVT reactions on *pagC* in the presence of 500 nM H-NS over a series of Mg^{2+} concentrations, ranging from 0.5 to 50 mM. Mg^{2+} was found to inhibit H-NS-mediated silencing in a continuous, linear manner, with silencing becoming undetectable at 50 mM $MgCl_2$ (Figure 1B). This observation does not support a model in which Mg^{2+} promotes a switch from one binding mode to another. Furthermore, the effect of Mg^{2+} on transcriptional regulation is at least partially specific to H-NS, as RNAP did not exhibit the same Mg^{2+} concentration-dependent response (Supplementary Figure S3).

Mg^{2+} concentration modulates H-NS binding affinity

We hypothesized that the Mg^{2+}-dependent modulation of silencing could be due to a structural change associated with conversion to bridging mode, or alternatively, Mg^{2+} could be inhibiting DNA binding by H-NS. To analyze the effect of Mg^{2+} concentration on H-NS–DNA interactions, we employed DNase I footprinting and differential DNA footprint analysis (DDFA), a highly-sensitive and quantitative method that allows the detection of DNA structural changes that might be associated with specific binding modes. Performance of DDFA over a range of H-NS concentrations allowed determination of the binding affinity of H-NS for the *pagC* promoter region at single base-pair resolution (Figure 2A, B; Supplementary Figure S4). H-NS was observed to bind extensively to a region upstream of the *pagC* promoter, from position –139 to –12 relative to the transcriptional start site (TSS). High affinity binding sites, based on fractional occupancy at low (20 nM) H-NS concentrations, are clustered relatively distal to the promoter, with strongest binding observed at positions –139, –119 and –114, whereas more proximal protected sites, such as –48 and –34, exhibited lower affinity and were not bound by 20 nM H-NS. As H-NS concentrations increased, the distal H-NS binding sites became saturated with H-NS, followed by binding sites more proximal to the promoter. Notably, an analysis of the *pagC* promoter region using the Virtual Footprint program (www.prodoric.de/vfp) (28) indicated that the best fits to the H-NS consensus binding site are centered at positions –121, –134 and –141 (Supplementary Figure S5), overlapping our observed high affinity sites. These results suggest that that H-NS initially nucleates at the promoter-distal region between –139 and –119, then oligomerizes towards the *pagC* promoter, binding lower affinity sites to silence transcription. The promoter-distal site is likely to represent the initial binding site of a single H-NS dimer, as structural studies indicate that an H-NS dimer occupies approximately two turns of the DNA helix, or 21 bp (8).

At a concentration of 10 mM Mg^{2+}, H-NS protected the same positions from DNase I digestion as observed in 1 mM Mg^{2+} (Figure 2B). However, affinity for H-NS was clearly reduced at the higher Mg^{2+} concentration (Figure 2C). Furthermore, the absence of any novel DNase I hypersensitive sites, as indicated by the peaks that are associated with DNA bending or distortion of the duplex (29,30), suggests that the DNA does not form structures unique to higher Mg^{2+} concentrations (Figure 2B). Rather, the general structure of the H-NS-bound *pagC* promoter complex appears to be similar under high and low Mg^{2+} concentrations. The difference in affinity is not an artifact resulting from altered DNase I activity, as DNase I control reactions did not exhibit significant differences when performed in either 1 or 10 mM Mg^{2+} (Supplementary Figure S6). Furthermore, as was observed in the IVT experiments, Mg^{2+}-dependent modulation of affinity was continuous and non-binary, as H-NS binding was completely inhibited at 50 mM Mg^{2+} (Figure 2D; Supplementary Figure S7).

These results indicate that Mg^{2+} does not control a binding-mode switch, but rather inhibits DNA binding by H-NS, and that the degree of binding determines the structure of the local H-NS–DNA complex and its ability to impede transcription. High-affinity interactions (Figure 2C, positions –139, –119) appear to be inhibited to a greater degree than low-affinity interactions (Figure 2C, positions –60, –12). This suggests that more than one region of H-NS is involved in high affinity interactions with DNA, and that one of these regions interacts with, and is subsequently inhibited by, Mg^{2+}. Furthermore, it also implies that this second region is unnecessary for low affinity interactions, which may promote bridging, and are unaffected by changes in Mg^{2+}. However, our IVT data (Figure 1) suggest that these low affinity interactions are insufficient for silencing. In support of this, Gao *et al.* (31) have recently observed that both the DNA binding domain and the linker region are required for high affinity interactions with DNA. It is therefore plausible that Mg^{2+} interferes with the ability of the linker to support high-affinity interactions and the formation of stiffened filaments. Notably, the linker is rich in negatively-charged glutamate residues, which can facilitate Mg^{2+} binding (8), providing several potential Mg^{2+}-binding sites. In particular, the E102 residue in the C-terminal DNA-binding domain undergoes a substantial chemical shift in response to DNA binding (4). Although E102 is not thought to be directly involved in DNA binding, it is conceivable that it coordinates Mg^{2+} binding and H-NS inhibition. Further investigation will be required to determine how the inhibition of H-NS binding occurs.

Binding mode is a function of H-NS concentration and affinity

To test the hypothesis that Mg^{2+} influences the affinity of the H-NS–DNA interaction rather than directly controlling the binding mode, we normalized the DDFA results to transcriptional silencing activity, rather than to H-NS concentration, under varying Mg^{2+} concentrations. Specifically, the structures of H-NS–DNA complexes exhibiting comparable levels of silencing in 1 or 10 mM MgCl$_2$ were compared. Transcription of *pagC* is silenced 6-fold in 200 nM H-NS and 1 mM MgCl$_2$, and 9-fold in 500 nM H-NS and 10 mM MgCl$_2$, respectively (Figure 1A). A DDFA comparison of these two complexes failed to identify any significant structural differences in the H-NS–DNA complex (Supplementary Figure S8). This suggests that H-NS–DNA complexes with equivalent silencing activity are structurally similar, regardless of the Mg^{2+} concentration present.

This was corroborated using UV laser photo-crosslinking (32) and AFM of H-NS-*pagC* promoter complexes in 1 or 10 mM Mg^{2+}. In UV laser photo-crosslinking, DNA is irradiated with brief (10 ns) pulses of UV irradiation at a wavelength of 266 nm, causing the formation of photo-crosslinks between adjacent thymidine residues in a structurally dependent manner, which can be analyzed via DDFA. This method is useful to detect alterations of DNA structure that result from protein binding. Target plasmid was incubated in the presence of increasing concentrations of H-NS in buffers containing 1 or 10 mM Mg^{2+}, and the resulting complexes were photo-crosslinked (Figure 3; Supplementary Figure S9). In both the 1 and 10 mM reactions, three significant valleys were detectable at positions –139, –77 and –43, indicating that the H-NS induces similar struc-
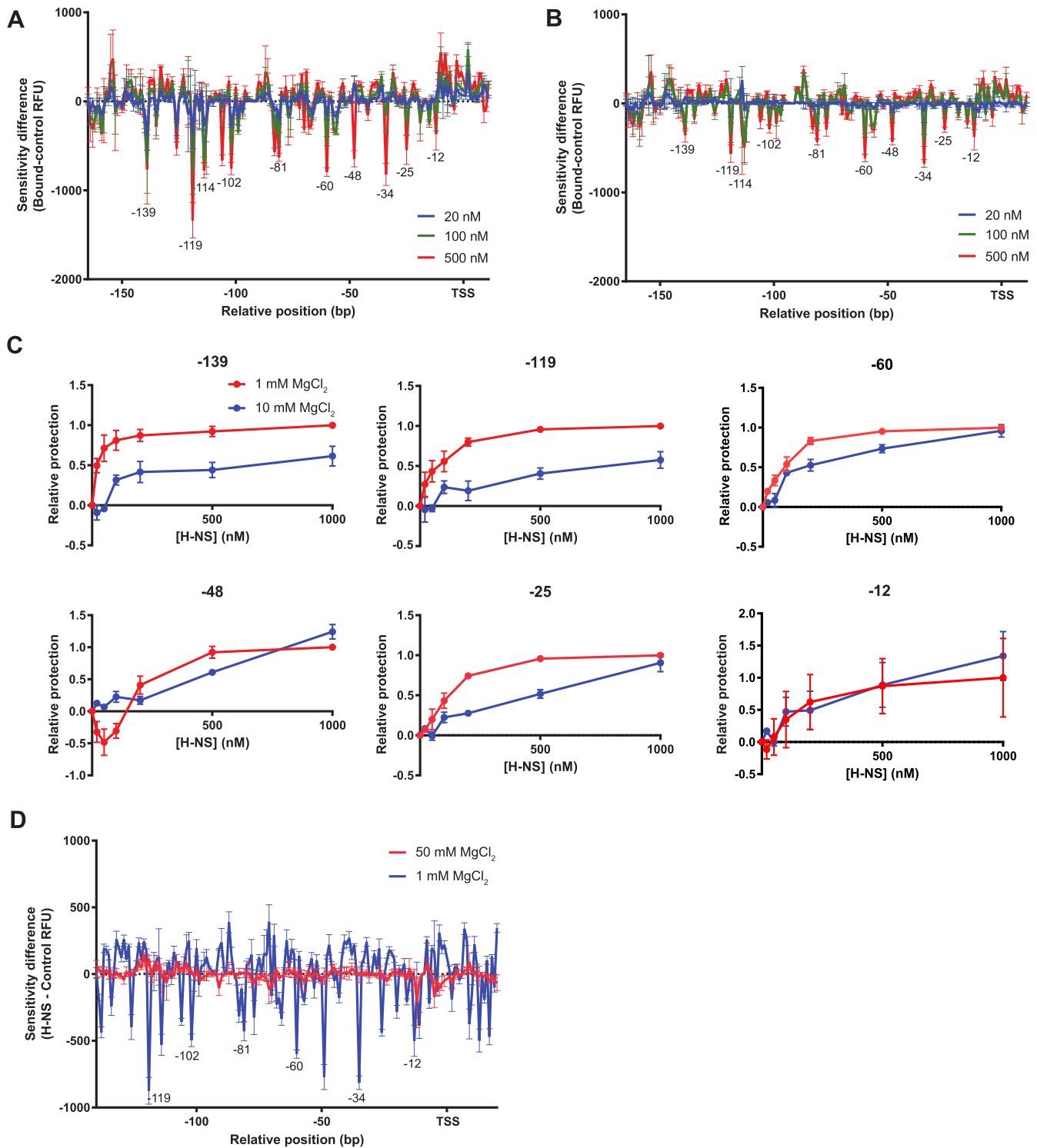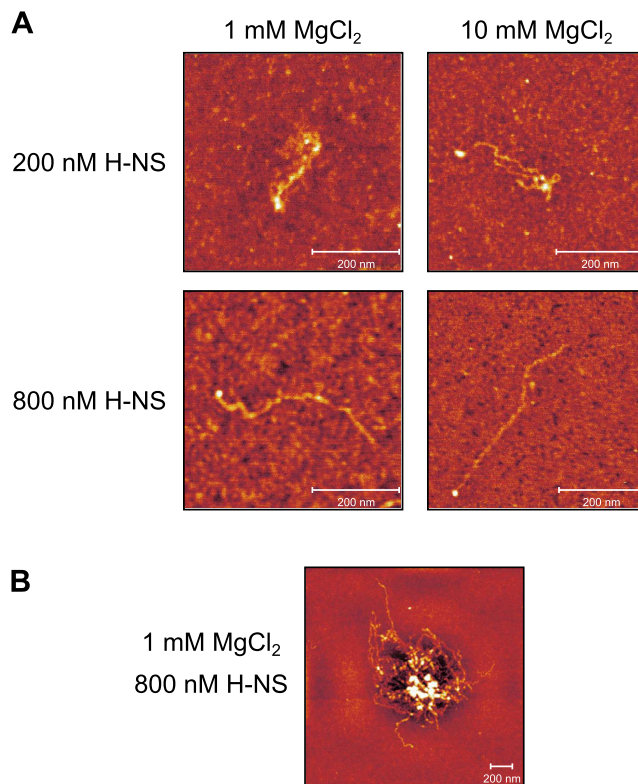
Figure 2. H-NS binding is inhibited by increasing Mg^{2+} concentrations. DNase I Differential DNA Footprint Analysis was performed on the *pagC* promoter region with increasing concentrations of H-NS under either stiffening (**A**; 1 mM $MgCl_2$) or bridging (**B**; 10 mM $MgCl_2$) conditions. Results are presented as DDFA plots, representing the difference in fluorescent peak height (relative fluorescence units; RFU) between the control and H-NS-bound samples at three different H-NS concentrations (20 nM; blue line, 100 nM; green line, and 500 nM; red line). The approximate position of nucleotides relative to the TSS is indicated on the horizontal axis. Data represent the mean ± SD; $n = 3$. Downward valleys are regions of protection from DNase I digestion, indicating protein binding, whereas upward peaks indicate regions of increased DNase I sensitivity, suggesting bending or distortion of the DNA duplex. See Supplementary Figure S4 for representative electropherograms. (**C**) The fractional protection of several bases (−139, −119, −60, −48, −25 and −12 relative to the TSS) was determined relative to the reaction conditions resulting in maximum protection (1000 nM H-NS and 1 mM $MgCl_2$) and plotted for a range of H-NS concentrations in either 1 mM (red line) or 10 mM (blue line) $MgCl_2$, indicating the approximate affinity of the interaction between each base and H-NS. (**D**) 50 mM $MgCl_2$ completely inhibited H-NS binding. DNase I DDFA was performed on the *pagC* promoter region in the presence of 500 nM H-NS and either 1 mM (blue line) or 50 mM (red line) $MgCl_2$.
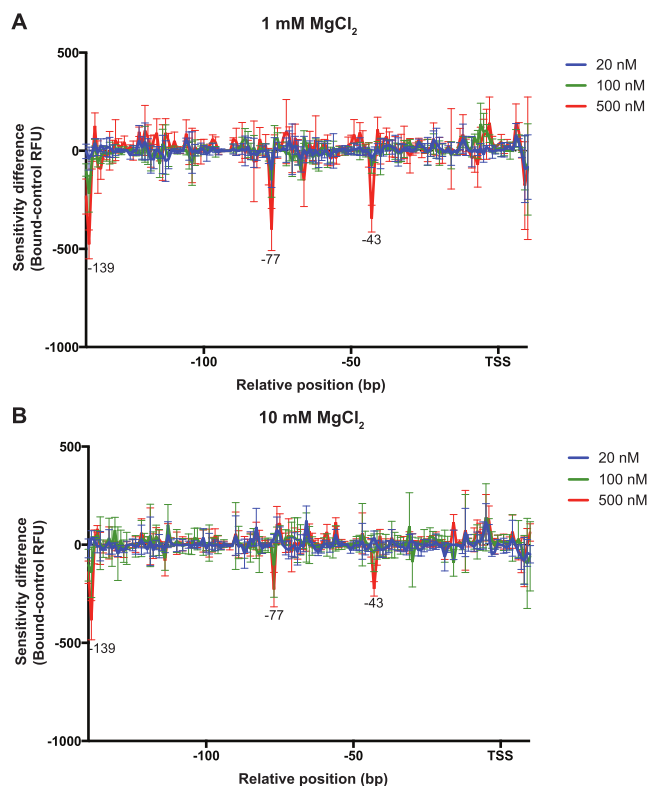
Figure 3. Local DNA structure is similar at low and high Mg^{2+} concentrations. UV laser Differential DNA Footprinting Analysis was performed on the *pagC* promoter region in increasing concentrations of H-NS under either stiffening (**A**; 1 mM $MgCl_2$) or bridging (**B**; 10 mM $MgCl_2$) conditions. Results are presented as DDFA plots, representing the difference in fluorescent peak height (relative fluorescence units; RFU) between control and H-NS-bound samples at three different H-NS concentrations (20 nM; blue line, 100 nM; green line and 500 nM; red line). The approximate position of cross-linked nucleotides relative to the TSS is indicated on the horizontal axis. Data represent the mean ± SD; $n = 3$. Significant cross-linking, suggestive of structural changes, is detectable at positions –139, –77 and –43. Representative electropherograms are shown in Supplementary Figure S7.

Figure 4. H-NS binding, but not binding mode, correlates with Mg^{2+} concentrations. The linearized 2.7 kb (~610 nm) *pagC* region was incubated in the presence of 1 or 10 mM $MgCl_2$, and 200 or 800 nM H-NS, at room temperature, and applied to glutaraldehyde-treated mica. H-NS-*pagC* complexes were then imaged by AFM in air. Representative discrete complexes are shown (**A**). At a concentration of 200 nM, which is sufficient for silencing (Figure 1), H-NS appears to form bridges in 1 mM $MgCl_2$ (see Supplementary Figure S10 for additional images of the bridged complex, as well as the unbound DNA control), but stiffened filaments form at 800 nM H-NS. Similarly, in 10 mM $MgCl_2$, H-NS binding is limited, but H-NS appears to form bridges when present at a concentration of 200 nM. However, filaments can be observed when the H-NS concentration is increased to 800 nM. Multimolecular aggregates, suggestive of bridging, can be observed under all binding conditions, but appear to be largest in 1 mM $MgCl_2$ and 800 nM H-NS (**B**). Observed binding modes are scored in Supplementary Figure S11. Representative aggregates are shown for all conditions in Supplementary Figure S12A. The diameters of observed aggregates, which are reflective of H-NS binding and oligomerization, are indicated in Supplementary Figure S12B.

tural changes to the DNA under both conditions. However, the magnitude of the peaks observed was smaller in 10 mM Mg^{2+}, further supporting an inverse correlation between Mg^{2+} concentration and H-NS binding affinity.

For AFM studies, a linearized version of the 2.7 kb *pagC* fragment was used to allow the appropriate orientation of the DNA and to identify the approximate location of *pagC*. H-NS-*pagC* complexes were formed with 200 and 800 nM H-NS in buffer containing either 1 or 10 mM Mg^{2+} (Figure 4A). In 1 mM Mg^{2+} and 200 nM H-NS, discrete H-NS-*pagC* complexes appear to adopt a bridged conformation, as the fragments are typically less than half their predicted length (~610 nm) (Supplementary Figures S10 and S11). This is further supported by the presence of what appear to be segments of unbridged DNA within some complexes (Supplementary Figure S10A, right panel). This contradicts the biphasic model, which precludes the formation of a bridged complex in 1 mM Mg^{2+}. However, in 800 nM H-NS, discrete H-NS-*pagC* complexes form filaments. In 10 mM Mg^{2+} and 200 nM H-NS, H-NS-*pagC* complexes form

disorganized interwound or bridged structures. In support of our IVT and DDFA results, very little H-NS appears to bind under these conditions; the complex is predominantly naked DNA. However, it becomes saturated in 800 nM H-NS, forming a stiffened filament. Again, this observation contradicts the biphasic model. Given these observations, we conclude that our DDFA data at lower concentrations represent a mixture of bridging and stiffening interactions, transitioning to more stiffening interactions as the H-NS concentration increases, saturating the DNA.

Under all of the conditions assayed above, disordered aggregates of H-NS and DNA were also observed (Figure 4B; Supplementary Figure S12). Because these aggregates consist of multiple DNA molecules, they must be the product of intra- and inter-molecular bridging interactions, as the stiffening mode would not promote the formation of such
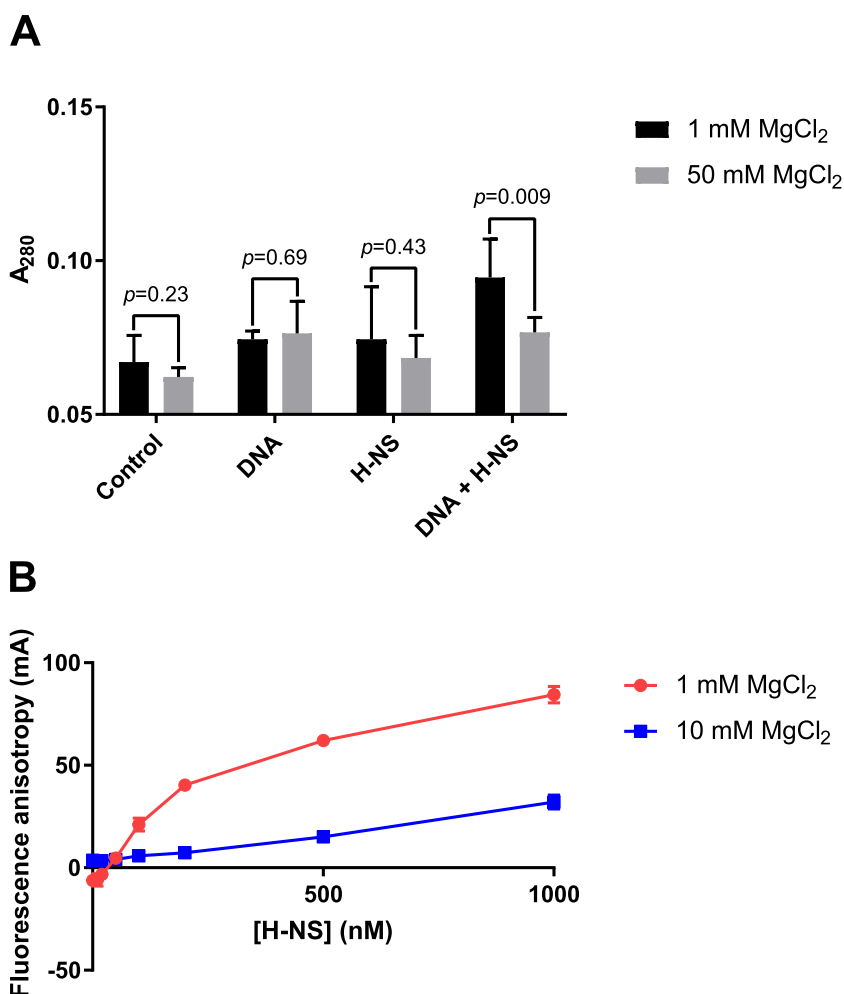
Figure 5. H-NS-mediated aggregation is dependent on DNA binding, which is inhibited by Mg^{2+}. The linearized 2.7 kb *pagC* region was incubated in the presence of 800 nM H-NS and either 1 or 50 mM $MgCl_2$. Light scattering, which is indicative of aggregate formation, was measured at 280 nm (**A**). An increase in light scattering was detected in samples containing both H-NS and DNA at 1 mM $MgCl_2$. However, a significant increase in light scattering was not detected in 50 mM $MgCl_2$, a concentration sufficient to inhibit DNA binding. This indicates that aggregation requires DNA binding, which is inhibited by $MgCl_2$. Data represent the mean $\pm$ SD; $n \geq 5$. *P*-values are indicated above each pair of samples. To confirm that $MgCl_2$ inhibits DNA binding directly, fluorescence anisotropy was performed using a 36bp target containing a high affinity H-NS binding site (**B**). 6-FAM-labeled DNA was incubated in the presence of increasing concentrations of H-NS and 1 or 10 mM $MgCl_2$, as indicated, and anisotropy, which is indicative of H-NS binding, was measured. Anisotropy is significantly decreased at 10 mM $MgCl_2$, indicating that $MgCl_2$ directly inhibits the H-NS–DNA interaction. Data represent the mean $\pm$ SD of three independent experiments, each consisting of three technical replicates. The anisotropy of the reaction buffer containing 1 mM $MgCl_2$ is subtracted from all samples to correct for background fluorescence.

complexes. Although the exact sizes of the aggregates are difficult to accurately quantify using these methods, their diameters appear to correlate with affinity as predicted under our model (Supplementary Figure S12B). Aggregates progressively increase in size from 10 mM Mg^{2+} and 200 nM H-NS, up to 1 mM Mg^{2+} and 800 nM H-NS, exhibiting the strongest binding under the latter conditions. We suggest that this reflects the dynamic nature of H-NS binding. When H-NS concentrations are high, an isolated DNA molecule will form a filament as it becomes saturated with H-NS. However, multiple DNA molecules will decrease the effective H-NS concentration, promoting bridging and the formation of aggregates. Previous magnetic tweezer experiments failed to observe aggregation because those assays contained a single DNA molecule (16), driving the complex to form a filament.

To determine whether this aggregation was a product of H-NS–DNA interactions or H-NS self-association, we performed light scattering analysis of H-NS–DNA complexes (Figure 5A; Supplementary Figure S13). The 2.7 kb *pagC* region was incubated in the presence of 800 nM H-NS and either 1 or 50 mM $MgCl_2$, the latter of which is sufficient to inhibit H-NS binding. Significant light scattering at 280 nm (Figure 5; Supplementary Figure S13) was detectable in samples containing DNA, H-NS and 1 mM $MgCl_2$. However, light scattering was inhibited by 50 mM $MgCl_2$. Aggregation is not due to H-NS self-association, as H-NS had no effect on light scattering in the absence of DNA, indicating that H-NS oligomerization is dependent on DNA binding and is inhibited by $MgCl_2$. We then used fluorescence anisotropy to determine whether $MgCl_2$ inhibits the H-NS–DNA interaction itself, or the oligomerization of H-NS

bound to DNA (Figure 5B). From our DNase I DDFA and Virtual Footprint data, we identified a 36 bp region centered at position –132 (Supplementary Figure S5) which binds H-NS with high affinity. Because structural data suggest that an H-NS dimer occupies >20 bp upon binding DNA (8), this target should accommodate only a single H-NS dimer and should not support significant oligomerization. We observed a direct relationship between the anisotropy of this fragment and the concentration of H-NS, indicating the formation of an H-NS–DNA complex. The change in anisotropy was inhibited by 10 mM $MgCl_2$, indicating that Mg^{2+} directly inhibits the H-NS–DNA interaction.

These observations were unexpected in view of the recently proposed models for H-NS–DNA interactions. However, several observations in the literature support the hypothesis that the higher-order structure of the H-NS–DNA complex is influenced by both DNA binding affinity and local H-NS concentration. An earlier biochemical analysis of H-NS (33) demonstrated that at low concentrations, H-NS constrains supercoils in plasmid DNA, suggestive of DNA bridging. However, as the H-NS concentration increased, the entire plasmid was bound and supercoils were no longer constrained, suggesting a transition to the stiffening mode. More recently, H-NS–DNA complexes were observed to switch from bridging to stiffening at increasing H-NS concentrations, even in the presence of 10 mM Mg^{2+} (21). Taken together with our present findings, these observations suggest that the observed switch between binding modes is not directly dependent on divalent cation concentration, but rather is a complex function of both the affinity of H-NS–DNA interactions and local H-NS concentrations (the number of H-NS molecules bound to a specific segment of DNA). As the affinity of H-NS–DNA interactions decreases, fewer H-NS molecules bind DNA, and those that do bind are isolated, without local interaction partners. Such isolated H-NS molecules must interact *in trans* with distant partners to form bridges. A similar model was recently proposed by Joyeux (34), who used computational modeling to analyze the interaction between H-NS and the bacterial chromosome in response to varying cation concentrations. That study proposed that divalent cations condense on the polyanionic phosphate backbone to inhibit H-NS–DNA interactions, and that increasing cation concentrations indirectly promote H-NS bridging interactions by reducing the affinity of DNA binding. Transcriptional silencing is also not directly associated with one binding mode or another *per se*, but rather, correlates with the degree of binding, which is greater under conditions associated with stiffening. It is important to note that free intracellular Mg^{2+} concentrations are tightly controlled by extracellular Mg^{2+}-uptake systems: in *Salmonella* these consist of CorA, MgtA and MgtB (35,36). Free $[Mg^{2+}]$ may vary by as little as 2-fold, irrespective of the magnitude of fluctuations in extracellular Mg^{2+} (19), which our observations suggest would result in a roughly two-fold change in H-NS activity. This limited effect makes it unlikely that Mg^{2+} plays a significant direct regulatory role. We suggest instead that the previously-reported Mg^{2+}-effect is a proxy for the affinity of the H-NS–DNA interaction, allowing us to probe the impact of affinity on H-NS–DNA binding, structure and activity.

Although previous studies suggest that the cytoplasmic concentration of H-NS is approximately 13 μM (37), which should be sufficient to promote filament formation, H-NS is unlikely to be homogeneously distributed throughout the cell. Computational studies predict the formation of 3D aggregates (34), similar to the complexes described here. Although chromosomal conformation studies have failed to identify H-NS-dependent pairwise interactions between distant bound loci (38), H-NS-bound regions may still coassociate in a less organized manner. Multiple studies have described the formation of distinct H-NS-associated foci in a growth rate- and phase-dependent manner (31,39,40). Therefore, local H-NS concentrations are likely to be variable throughout the nucleoid, and both binding modes are likely to occur in the cell. This suggests a basis for the role of H-NS in organizing higher-order bacterial chromatin structure, as less densely-bound regions may not have direct regulatory importance but might form bridges to condense the bacterial nucleoid (39,41,42). Other physiological stimuli that are known to impact H-NS activity, such as pH, temperature and osmolarity (43–45), may similarly modulate H-NS binding. Notably, alkaline pH and elevated temperatures have also been observed to promote bridging (16). It seems likely that these conditions are acting by reducing the affinity of H-NS–DNA interactions, allowing H-NS to influence bacterial chromatin structure and global gene expression in response to numerous environmental signals.

SUPPLEMENTARY DATA

Supplementary Data are available at NAR Online.

REFERENCES

1. Navarre,W.W., Porwollik,S., Wang,Y., McClelland,M., Rosen,H., Libby,S.J. and Fang,F.C. (2006) Selective silencing of foreign DNA with low GC content by the H-NS protein in *Salmonella*. *Science*, **313**, 236–238.
2. Lucchini,S., Rowley,G., Goldberg,M.D., Hurd,D., Harrison,M. and Hinton,J.C. (2006) H-NS mediates the silencing of laterally acquired genes in bacteria. *PLoS Pathog.*, **2**, e81.
3. Will,W.R., Navarre,W.W. and Fang,F.C. (2015) Integrated circuits: how transcriptional silencing and counter-silencing facilitate bacterial evolution. *Curr. Opin. Microbiol.*, **23**, 8–13.

4. Gordon,B.R., Li,Y., Cote,A., Weirauch,M.T., Ding,P., Hughes,T.R., Navarre,W.W., Xia,B. and Liu,J. (2011) Structural basis for recognition of AT-rich DNA by unrelated xenogeneic silencing proteins. *Proc. Natl. Acad. Sci. U.S.A.*, **108**, 10690–10695.

5. Stella,S., Spurio,R., Falconi,M., Pon,C.L. and Gualerzi,C.O. (2005) Nature and mechanism of the *in vivo* oligomerization of nucleoid protein H-NS. *EMBO J.*, **24**, 2896–2905.

6. Esposito,D., Petrovic,A., Harris,R., Ono,S., Eccleston,J.F., Mbabaali,A., Haq,I., Higgins,C.F., Hinton,J.C., Driscoll,P.C. *et al.* (2002) H-NS oligomerization domain structure reveals the mechanism for high order self-association of the intact protein. *J. Mol. Biol.*, **324**, 841–850.

7. Leonard,P.G., Ono,S., Gor,J., Perkins,S.J. and Ladbury,J.E. (2009) Investigation of the self-association and hetero-association interactions of H-NS and StpA from Enterobacteria. *Mol. Microbiol.*, **73**, 165–179.

8. Arold,S.T., Leonard,P.G., Parkinson,G.N. and Ladbury,J.E. (2010) H-NS forms a superhelical protein scaffold for DNA condensation. *Proc. Natl. Acad. Sci. U.S.A.*, **107**, 15728–15732.

9. Grainger,D.C. (2016) Structure and function of bacterial H-NS protein. *Biochem. Soc. Trans.*, **44**, 1561–1569.

10. Bloch,V., Yang,Y., Margeat,E., Chavanieu,A., Augé,M.T., Robert,B., Arold,S., Rimsky,S. and Kochoyan,M. (2003) The H-NS dimerization domain defines a new fold contributing to DNA recognition. *Nat. Struct. Biol.*, **10**, 212–218.

11. Cerdan,R., Bloch,V., Yang,Y., Bertin,P., Dumas,C., Rimsky,S., Kochoyan,M. and Arold,S.T. (2003) Crystal structure of the N-terminal dimerisation domain of VicH, the H-NS-like protein of *Vibrio cholerae*. *J. Mol. Biol.*, **334**, 179–185.

12. Will,W.R., Bale,D.H., Reid,P.J., Libby,S.J. and Fang,F.C. (2014) Evolutionary expansion of a regulatory network by counter-silencing. *Nat. Commun.*, **5**, 5270.

13. Dame,R.T., Wyman,C. and Goosen,N. (2000) H-NS mediated compaction of DNA visualised by atomic force microscopy. *Nucleic Acids Res.*, **28**, 3504–3510.

14. Dame,R.T., Noom,M.C. and Wuite,G.J. (2006) Bacterial chromatin organization by H-NS protein unravelled using dual DNA manipulation. *Nature*, **444**, 387–390.

15. Amit,R., Oppenheim,A.B. and Stavans,J. (2003) Increased bending rigidity of single DNA molecules by H-NS, a temperature and osmolarity sensor. *Biophys. J.*, **84**, 2467–2473.

16. Liu,Y., Chen,H., Kenney,L.J. and Yan,J. (2010) A divalent switch drives H-NS/DNA-binding conformations between stiffening and bridging modes. *Genes Dev.*, **24**, 339–344.

17. Moncany,M.L. and Kellenberger,E. (1981) High magnesium content of *Escherichia coli* B. *Experientia*, **37**, 846–847.

18. Alatossava,T., Jütte,H., Kuhn,A. and Kellenberger,E. (1985) Manipulation of intracellular magnesium content in polymyxin B nonapeptide-sensitized *Escherichia coli* by ionophore A23187. *J. Bacteriol.*, **162**, 413–419.

19. Froschauer,E.M., Kolisek,M., Dieterich,F., Schweigel,M. and Schweyen,R.J. (2004) Fluorescence measurements of free $[Mg^{2+}]$ by use of mag-fura 2 in *Salmonella enterica*. *FEMS Microbiol. Lett.*, **237**, 49–55.

20. Lim,C.J., Lee,S.Y., Kenney,L.J. and Yan,J. (2012) Nucleoprotein filament formation is the structural basis for bacterial protein H-NS gene silencing. *Sci. Rep.*, **2**, 509.

21. Kotlajich,M.V., Hron,D.R., Boudreau,B.A., Sun,Z., Lyubchenko,Y.L. and Landick,R. (2015) Bridged filaments of histone-like nucleoid structuring protein pause RNA polymerase and aid termination in bacteria. *Elife*, **4**, e04970.

22. Perez,J.C., Latifi,T. and Groisman,E.A. (2008) Overcoming H-NS-mediated transcriptional silencing of horizontally acquired genes by the PhoP and SlyA proteins in *Salmonella enterica*. *J. Biol. Chem.*, **283**, 10773–10783.

23. Wang,R.F. and Kushner,S.R. (1991) Construction of versatile low-copy-number vectors for cloning, sequencing and gene expression in *Escherichia coli*. *Gene*, **100**, 195–199.

24. Aparicio,O., Geisberg,J.V., Sekinger,E., Yang,A., Moqtaderi,Z. and Struhl,K. (2005) Chromatin immunoprecipitation for determining the association of proteins with specific genomic sequences *in vivo*. *Curr. Protoc. Mol. Biol.*, doi:10.1002/0471143030.cb1707s23.

25. Shlyakhtenko,L.S., Gall,A.A. and Lyubchenko,Y.L. (2013) Mica functionalization for imaging of DNA and protein-DNA complexes with atomic force microscopy. *Methods Mol. Biol.*, **931**, 295–312.

26. Wang,H., Bash,R., Yodh,J.G., Hager,G.L., Lohr,D. and Lindsay,S.M. (2002) Glutaraldehyde modified mica: a new surface for atomic force microscopy of chromatin. *Biophys. J.*, **83**, 3619–3625.

27. van der Maarel,J.R., Guttula,D., Arluison,V., Egelhaaf,S.U., Grillo,I. and Forsyth,V.T. (2016) Structure of the H-NS–DNA nucleoprotein complex. *Soft Matter*, **12**, 3636–3642.

28. Münch,R., Hiller,K., Grote,A., Scheer,M., Klein,J., Schobert,M. and Jahn,D. (2005) Virtual Footprint and PRODORIC: an integrative framework for regulon prediction in prokaryotes. *Bioinformatics*, **21**, 4187–4189.

29. Drew,H.R. and Travers,A.A. (1984) DNA structural variations in the *E. coli tyrT* promoter. *Cell*, **37**, 491–502.

30. Suck,D., Lahm,A. and Oefner,C. (1988) Structure refined to 2A of a nicked DNA octanucleotide complex with DNase I. *Nature*, **332**, 464–468.

31. Gao,Y., Foo,Y.H., Winardhi,R.S., Tang,Q., Yan,J. and Kenney,L.J. (2017) Charged residues in the H-NS linker drive DNA binding and gene silencing in single cells. *Proc. Natl. Acad. Sci. U.S.A.*, **114**, 12560–12565.

32. Buckle,M., Geiselmann,J., Kolb,A. and Buc,H. (1991) Protein-DNA cross-linking at the *lac* promoter. *Nucleic Acids Res.*, **19**, 833–840.

33. Tupper,A.E., Owen-Hughes,T.A., Ussery,D.W., Santos,D.S., Ferguson,D.J., Sidebotham,J.M., Hinton,J.C. and Higgins,C.F. (1994) The chromatin-associated protein H-NS alters DNA topology *in vitro*. *EMBO J.*, **13**, 258–268.

34. Joyeux,M. (2018) Role of salt valency in the switch of H-NS proteins between DNA-bridging and DNA-stiffening modes. *Biophys. J.*, **114**, 1–9.

35. Smith,R.L. and Maguire,M.E. (1998) Microbial magnesium transport: unusual transporters searching for identity. *Mol. Microbiol.*, **28**, 217–226.

36. Snavely,M.D., Florer,J.B., Miller,C.G. and Maguire,M.E. (1989) Magnesium transport in *Salmonella typhimurium*: $^{28}Mg^{2+}$ transport by the CorA, MgtA, and MgtB systems. *J. Bacteriol.*, **171**, 4761–4766.

37. Azam,T.A. and Ishihama,A. (1999) Twelve species of the nucleoid-associated protein from *Escherichia coli*. Sequence recognition specificity and DNA binding affinity. *J Biol Chem*, **274**, 33105–33113.

38. Cagliero,C., Grand,R.S., Jones,M.B., Jin,D.J. and O'Sullivan,J.M. (2013) Genome conformation capture reveals that the *Escherichia coli* chromosome is organized by replication and transcription. *Nucleic Acids Res.*, **41**, 6058–6071.

39. Wang,W., Li,G.W., Chen,C., Xie,X.S. and Zhuang,X. (2011) Chromosome organization by a nucleoid-associated protein in live bacteria. *Science*, **333**, 1445–1449.

40. Liu,Y., Xie,P., Wang,P., Li,M., Li,H., Li,W. and Dou,S. (2015) A model for chromosome organization during the cell cycle in live *E. coli*. *Sci. Rep.*, **5**, 17133.

41. Spassky,A., Rimsky,S., Garreau,H. and Buc,H. (1984) H1a, an *E. coli* DNA-binding protein which accumulates in stationary phase, strongly compacts DNA *in vitro*. *Nucleic Acids Res.*, **12**, 5321–5340.

42. Spurio,R., Dürrenberger,M., Falconi,M., La Teana,A., Pon,C.L. and Gualerzi,C.O. (1992) Lethal overproduction of the *Escherichia coli* nucleoid protein H-NS: ultramicroscopic and molecular autopsy. *Mol. Gen. Genet.*, **231**, 201–211.

43. Atlung,T. and Ingmer,H. (1997) H-NS: a modulator of environmentally regulated gene expression. *Mol. Microbiol.*, **24**, 7–17.

44. McLeod,S.M. and Johnson,R.C. (2001) Control of transcription by nucleoid proteins. *Curr. Opin. Microbiol.*, **4**, 152–159.

45. Williams,R.M. and Rimsky,S. (1997) Molecular aspects of the *E. coli* nucleoid protein, H-NS: a central controller of gene regulatory networks. *FEMS Microbiol. Lett.*, **156**, 175–185.